Proceedings World Geothermal Congress 2020+1
Reykjavik, Iceland, April - October 2021

Investigating Different Formulations for Hydrothermal Convection in Geothermal Systems

Po-Wei Huang[a,b*] and Florian Wellmann[b]

[a] Geothermal Energy and Geofluids Group, Department of Earth Sciences, ETH Zürich, 8092 Zürich, Switzerland

[b] Computational Geoscience and Reservoir Engineering, Jülich-Aachen Research Alliance (JARA-HPC), RWTH Aachen University, 52062, Aachen, Germany

[*] Previously affiliated at

powei.huang@erdw.ethz.ch, wellmann@aices.rwth-aachen.de

Keywords: Hydrothermal Convection, Reservoir Engineering, Pattern Formation

ABSTRACT

Hydrothermal convection in porous media is an essential piece of physics in geothermal reservoirs, and understanding them leads to better development of geothermal energy. We analyze the validity of simulating hydrothermal convection using different formulations of partial differential equations. Using the Elder problem as a benchmark, we found out that the stream function formulation and the velocity formulation are a valid and efficient model of hydrothermal convection. The Nusselt number is a measurement of the quality of convective heat transfer. The Rayleigh number describes the physical properties of porous media. We use simulations to investigate further the discrepancy in the Nusselt-Rayleigh relationship found in previous experiments. The conclusion is that the multiple steady-states of convection patterns in a 3D box are the main reason for the discrepancy found in the Nusselt-Rayleigh relationship.

1. INTRODUCTION

Consider a geothermal reservoir as a box full of porous media heated from below. Natural convection is the dominant driving force of fluids in such a system. For instance, the up-flow of hot fluids can cause shallow-high temperature anomalies. Due to this effect, the high-temperature region is closer to the surface. Therefore, the upflow region of natural convection is preferential for drilling and geothermal exploitation. At present, most conventional geothermal systems operate on such hydrothermal convective systems. A better understanding of natural convection in porous media can lead us to better decisions concerning designing injection and reinjection strategies of a geothermal power plant.

Therefore, we investigate the validity of different partial differential equations that model the natural convection problem. Can the modified equation solve the same physical problem? Can we use different formulations of the same equation to achieve more efficient simulations? We answer these questions using various benchmarks. Our goal is to build an efficient simulation tool that deals with large or maybe previously unsolvable problems.

Modeling natural convection in geothermal systems has become more prevalent. Lipsey et al. (2016) performed numerical simulations of thermal convection in the Luttelgeest carbonate platform and calibrated different models that match the observed temperature data. Niederau et al. (2017) compared simulations of thermal convection in the Perth Basin using homogeneous and heterogeneous permeability scenarios. Straus and Schubert (1979) found out multiple steady-states of convection patterns exist in a 3D box and suggested further research in the indeterminacy of steady-states using a probabilistic manner. The results of the above-mentioned research all showed the unpredictability of natural convection, that the convection pattern can change greatly by perturbing the state of the system (permeability, heterogeneity, the height of the reservoir, boundary conditions, etc.).

Compared to a conductive system, a convective system has a higher capability of heat transfer. A qualitative measure of the quality of convective heat transfer is the Nusselt number (Nu), which is the ratio of convective heat transfer to conductive heat transfer. The straightforward question would be: "Given a geothermal reservoir, how well can it transfer heat to the surface?" We use the Rayleigh number to quantify the combined characteristics of any given reservoir, under physical assumptions mentioned in Horne (1979):

- The Boussinesq assumption.
- Inertial effects are small, low Reynolds number.
- Viscosity is constant.
- Thermal dispersion is negligible.
- Saturating fluid and porous solid are in thermal equilibrium.

Experiments that investigate the relationship between the Nusselt number and the Rayleigh number (abbreviated as *Nu-Ra* relation) are performed using the Hele-Shaw cell analogy [Elder (1967a)] or a box full of porous media heated from below [Schneider (1963)] [Yen (1974)] [Kaneko et al. (1974)] [Combarnous and Bories (1975)] [Buretta and Berman (1976)]. Numerical experiments are performed to investigate the upper bound of the *Nu-Ra* relation [Combarnous and Bia (1971)] [Gupta and Joseph (1973)] [Straus (1974)] [Otero et al. (2004)]. Cheng (1979) compiled the *Nu-Ra* relation from some of the previously mentioned research papers, and the results are scattering even in the region of low Rayleigh number ($Ra<200$).

In a 3D box filled with saturated porous media, convection can happen in a two or three-dimensional setting. Straus and Schubert (1979) found out that two-dimensional flows have larger Nusselt numbers than three-dimensional flows when $Ra \leq 97$ using numerical simulations, and vice versa for $Ra>97$. The numerical simulations of Holst and Aziz (1972) and Horne (1979) also produced this effect. If both two and three-dimensional convection can exist in a box filled with porous media, then the system can at least have two Nusselt numbers. The result of Straus and Schubert (1979) indicates that it is always possible to force either steady two-

dimensional or steady three-dimensional convection by proper choice of initial conditions and that random initial conditions lead to either steady two-dimensional or steady three-dimensional convection. Beck (1972) showed that different box sizes favor 2D or 3D convection patterns using analytical methods.

Lister (1990) performed experiments using a large porous slab with two different porous media (a matrix of rubberized curled coconut fiber and clear polymethylmethacrylate beads) and concluded that the discrepancy of the *Nu-Ra* relation is caused by lateral thermal dispersion. Vadasz (2010) uses an analytical technique to explain the discrepancy of the *Nu-Ra* relation and concluded that weak boundary and domain imperfections are the reasons for the widespread relation. Lister (1990) and Vadasz (2010) explain this discrepancy from an experimental point of view, that we cannot perform perfect experiments. Therefore, we use simulations to overcome these experimental imperfections. We would like to propose a new explanation for the *Nu-Ra* relation using simulations.

We hypothesize that the discrepancy of the *Nu-Ra* relation is not only caused by lateral thermal dispersion and boundary imperfections but also caused by the multiple steady-states of convection patterns. Börsing et al. (2017) observed multiple possible convection modes in 2D boxes at the Rayleigh number regime above the critical Rayleigh number. Kimura et al. (2016) performed simulations in a 2D box and plotted the *Nu-Ra* relation with different convection modes when $100 \leq Ra \leq 400$. We investigate the *Nu-Ra* relation in a 3D box using the proposed finite element solver.

Different convection patterns give us a different quality of heat transfer. In a geothermal production setting, it is beneficial to enhance the Nusselt number. Using a injection-production doublet problem, we briefly investigate the possibility of changing convection patterns by velocity field perturbations. In the following sections, we discuss the detailed setup of the simulations and various benchmarks in section 2. The Nusselt-Rayleigh relationship and the results of the doublet problem are presented in section 3. Section 4 and 5 are dedicated to the discussion of the results and the conclusion of this work, respectively.

2. MATERIALS AND METHOD

2.1 Governing Equations

In this section, we introduce mass, momentum and energy conservation laws that describe natural convection in porous media.

2.1.1 Mass Conservation

We assume the fluid in the reservoir is single phase and incompressible. This incompressibility of fluid is also the result of the Boussinesq approximation. We introduce this divergence-free condition of the Darcy velocity q

$$\nabla \cdot q = 0,$$

$$q = \phi v,$$

$$q = (u, v, w),$$

where ϕ is the porosity, v is the seepage velocity. The Darcy velocity composes of three components u, v and w, which are the Darcy velocity in x, y and z directions, respectively.

2.1.2 Momentum Conservation

Darcy's law is suitable for modeling fluid flow in porous media, such as groundwater or geothermal reservoirs. It defines a relation between the pressure p and the Darcy velocity q. Geothermal reservoirs, particularly those found in volcanic rocks, are frequently highly fractured, and for many purposes, the fracturing is sufficiently dense and pervasive on a field scale such that the medium is considered homogeneous [Grant and Bixley (2011)]. Therefore, we introduce the generalization of Darcy's law in an isotropic and homogeneous medium [Bear (1972)]

$$q = -\frac{K}{\mu}(\nabla p - \rho_f g),$$

where K is the permeability of the reservoir, μ is the dynamic viscosity of the fluid and g is the gravity.

2.1.3 Energy Conservation

An advection-diffusion equation is used to model the transport of temperature T. We assume a simple situation in which the medium is isotropic and where radiative effects, viscous dissipation, the work done by pressure changes are negligible, and there is a local thermal equilibrium of solid and fluid phases [Nield and Bejan (2017)].

$$\frac{\partial}{\partial t}((\rho c)_m T) + q \cdot \nabla(\rho_f c_f T) - \nabla \cdot (k_m \nabla T) = 0,$$

$$(\rho c)_m = (1-\phi)\rho_s c_s + \phi \rho_f c_f,$$

$$k_m = (1-\phi)k_s + \phi k_f,$$

where $(\rho c)_m$ is the overall heat capacity per unit volume, and k_m is the overall thermal conductivity. The subscript s and f refers to solid and fluid, respectively.

2.1.4 Equation of State

We introduce an equation of state that couples fluid density and temperature

$$\rho_f = \rho_0(1 - \alpha(T - T_0)),$$

where ρ_0 is the fluid density at some reference temperature T_0, and α is the coefficient of thermal expansion. We assume the dynamic viscosity of fluid μ is constant.

2.2 Nondimensionalized Equations

There are many good analytical and numerical reasons for using nondimensionalized equations with proper scaling. The idea on which dimensional analysis is based is very simple, and can be understood by everybody: physical laws do not depend on arbitrarily chose basic units of measurement [Barenblatt (1996)]. Nowadays, the greatest practical benefit of scaling is related to running numerical simulations, since scaling greatly simplifies the choice of values for the input data and makes the simulation result more widely applicable [Langtangen and Pedersen (2016)]. Due to the finite representation and nonuniform distribution of floating-point values [Goldberg (1991)], it is, in general, better to scale the problem such that the quantities entering the computations are of unit size (or at least moderate) instead of being very large or very small [Langtangen and Pedersen (2016)].

We follow the derivation by Fowler (1997) closely, with changes in the scaling of pressure p, and the Darcy velocity q. The scaling factors are chosen such that the momentum equation and the energy equation both share some part of the dimensionless number

$$[p] = \sqrt{\frac{\mu d\alpha(\Delta T)gk_m}{c_f K}}, \quad [q] = \sqrt{\frac{K\alpha(\Delta T)gk_m}{\mu c_f d}}, \quad [t] = \frac{(\rho c)_{m0} d^2}{k_m},$$

$$T = T_0 + (\Delta T)T^*,$$

$$(\rho c)_{m0} = (1 - \phi)\rho_s c_s + \phi\rho_0 c_f,$$

where ΔT is the temperature difference between the top and bottom boundaries of the reservoir and d is the depth of the reservoir. The nondimensionalized equations are

$$\nabla \cdot q = 0, \tag{1}$$

$$q = -\nabla p + \sqrt{Ra}\, T\hat{j}, \tag{2}$$

$$T_t + \sqrt{Ra}\, q \cdot \nabla T - \nabla^2 T = 0, \tag{3}$$

$$Ra = \frac{(\rho_0)^2 g\alpha K d(\Delta T)c_f}{\mu k_m},$$

where Ra is the Rayleigh number. We abbreviated the partial derivatives w.r.t time by a subscript of t. In the following subsubsections, we review various formulations that solve the natural convection problem.

2.2.1 The Pressure Formulation

A direct way to solve the system of equations is to plug Darcy's law Eq. (2) into the divergence-free condition Eq. (1)

$$\nabla \cdot (-\nabla p + \sqrt{Ra}\, T\hat{j}) = 0.$$

Exchange the Darcy velocity term in Eq. (3) by Darcy's law Eq. (2), and we have the system of equations that couples pressure and temperature

$$T_t - \sqrt{Ra}\, \nabla p \cdot \nabla T + Ra\, T \frac{\partial T}{\partial y} - \nabla^2 T = 0.$$

Even though we try to separate the Rayleigh number into two equations by choosing appropriate scalings, it remains in the convection term in the y-direction. In a finite element solver, the mesh should be refined enough such that numerical oscillations of temperature do not appear. Furthermore, in the variational form of the pressure diffusion equation, the no-flux boundary condition is only weakly imposed. Horne (1979) compared finite difference implementations between the pressure formulation and the velocity potential formulation (which we refer to as the stream function formulation) and found out that the latter can be solved much faster and more accurate. Therefore, the pressure formulation is presented here only for completeness. It will not appear in further discussions.

2.2.2 The Stream Function Formulation

The derivation of the stream function formulation closely follows the Ph.D. thesis of Horne (1975). In natural convection problems, pressure boundary conditions are hard to define. Thus we define a stream function ψ that automatically satisfies the divergence-free condition of the Darcy flux

$$u = \frac{\partial \psi}{\partial y}, \; v = -\frac{\partial \psi}{\partial x}.$$

Curl Eq. (2)

Huang and Wellmann.

$$\nabla \times q = \nabla \times (-\nabla p + \sqrt{Ra}\, T\hat{j}). \tag{4}$$

Expand and multiply Eq. (4) by -1

$$\frac{\partial u}{\partial y} - \frac{\partial v}{\partial x} + \sqrt{Ra}\frac{\partial T}{\partial x} = 0. \tag{5}$$

Replace the Darcy fluxes in Eq. (5) and Eq. (3) by the stream function ψ

$$\frac{\partial^2 \psi}{\partial x^2} + \frac{\partial^2 \psi}{\partial y^2} + \sqrt{Ra}\frac{\partial T}{\partial x} = 0,$$

$$T_t + \sqrt{Ra}\left(\frac{\partial \psi}{\partial y}\frac{\partial T}{\partial x} - \frac{\partial \psi}{\partial x}\frac{\partial T}{\partial y}\right) - \nabla^2 T = 0.$$

This is the stream function formulation in 2D. The boundary conditions for a confined box are simple, $\psi = 0$ on the top, bottom, left and right boundaries. We derive the stream function formulation in 3D, followed by Horne (1979) and Hewitt et. al. (2014). Expand Eq. (4) in 3D with three Darcy velocity components (u, v, w)

$$\frac{\partial w}{\partial y} - \frac{\partial v}{\partial z} = -\sqrt{Ra}\frac{\partial T}{\partial z},$$

$$\frac{\partial u}{\partial z} - \frac{\partial w}{\partial x} = 0, \tag{6}$$

$$\frac{\partial v}{\partial x} - \frac{\partial u}{\partial y} = \sqrt{Ra}\frac{\partial T}{\partial x}.$$

Define a stream function $\psi = (\psi_1, 0, \psi_2)$ which is divergence-free

$$q = \nabla \times \psi,$$

$$\nabla \cdot \psi = 0. \tag{7}$$

Exchange the Darcy velocity by stream functions in Eq. (6), and invoke the divergence-free condition of the stream functions Eq. (7)

$$-\nabla^2 \psi_1 = -\sqrt{Ra}\frac{\partial T}{\partial z},$$

$$-\nabla^2 \psi_2 = \sqrt{Ra}\frac{\partial T}{\partial x}.$$

Substitute the Darcy velocities in Eq. (3) with the stream functions

$$T_t + \sqrt{Ra}\left(\frac{\partial \psi_2}{\partial y}\frac{\partial T}{\partial x} + \left(\frac{\partial \psi_1}{\partial z} - \frac{\partial \psi_2}{\partial x}\right)\frac{\partial T}{\partial y} - \frac{\partial \psi_1}{\partial y}\frac{\partial T}{\partial z}\right) - \nabla^2 T = 0.$$

For a confined box, the boundary conditions of the stream functions are straightforward

$\psi_1 = 0$, on $z = 0{,}1$ and $y = 0{,}1$,

$\psi_2 = 0$, on $x = 0{,}1$ and $y = 0{,}1$.

However, when there is production or injection of fluids into the box, the boundary conditions of stream functions are not that easy to define. Therefore, we introduce the velocity formulation, which solves the Darcy velocities directly.

2.2.3 The Velocity Formulation

This derivation is followed by Beck (1972), Florio (2014), Grodzka-Łukaszewska et. al. (2017). Instead of defining a stream function, we directly combine the divergence-free condition Eq. (1) and the vorticity equation Eq. (4) to form a velocity based formulation. Partially differentiate the vorticity equation Eq. (5) with respect to *x* and *y*

$$\frac{\partial^2 u}{\partial x \partial y} - \frac{\partial^2 v}{\partial x^2} + \sqrt{Ra}\frac{\partial^2 T}{\partial x^2} = 0,$$

$$\frac{\partial^2 u}{\partial y^2} - \frac{\partial^2 v}{\partial x \partial y} + \sqrt{Ra}\frac{\partial^2 T}{\partial x \partial y} = 0.$$

Partially differentiate the divergence-free condition Eq. (1) with respect to *x* and *y*, and rearrange

$$\frac{\partial^2 v}{\partial x \partial y} = -\frac{\partial^2 u}{\partial x^2},$$

$$\frac{\partial^2 u}{\partial x \partial y} = -\frac{\partial^2 v}{\partial y^2}.$$

Exchange the cross differentiation terms

$$\nabla^2 u + \sqrt{Ra}\frac{\partial^2 T}{\partial x \partial y} = 0,$$

$$\nabla^2 v - \sqrt{Ra}\frac{\partial^2 T}{\partial x^2} = 0.$$

Combined with Eq. (3), we have the 2D velocity formulation. The 3D velocity formulation can be obtained using the same technique. They are

$$\nabla^2 u + \sqrt{Ra}\ \frac{\partial^2 T}{\partial x \partial y} = 0,$$

$$\nabla^2 v - \sqrt{Ra}\ \left(\frac{\partial^2 T}{\partial x^2} + \frac{\partial^2 T}{\partial z^2}\right) = 0,$$

$$\nabla^2 w + \sqrt{Ra}\ \frac{\partial^2 T}{\partial y \partial z} = 0.$$

The boundary conditions of a confined box are straightforward. The velocity formulation allows us to set inflow and outflow boundary conditions easily.

2.3 Finite Element Methods and Variational Formulations

We solve the stream function formulation and the velocity formulation using MOOSE Framework [Gaston et al. (2009)], a finite element solver. The weak form is formulated by multiplying the partial differential equations by a test function ω and integrating over the computational domain Ω.

The weak form of the stream function formulation in 2D is

$$\int_\Omega (\nabla \omega \cdot \nabla \psi + \sqrt{Ra}\ \frac{\partial \omega}{\partial x}\ T) d\Omega = 0,$$

$$\int_\Omega \omega T_t d\Omega + \sqrt{Ra}\int_\Omega \omega \left(\frac{\partial \psi}{\partial y}\frac{\partial T}{\partial x} - \frac{\partial \psi}{\partial x}\frac{\partial T}{\partial y}\right) d\Omega + \int_\Omega \nabla \omega \cdot \nabla T d\Omega = 0.$$

We have to add a divergence-free condition of the stream functions ψ_1 and ψ_2 for the stream function formulation in 3D. Therefore, the weak form of the stream function formulation in 3D is

$$\int_\Omega \omega \left(\frac{\partial \psi_1}{\partial x} + \frac{\partial \psi_2}{\partial z}\right) d\Omega = 0,$$

$$\int_\Omega (\nabla \omega \cdot \nabla \psi_1 - \sqrt{Ra}\ \frac{\partial \omega}{\partial z}\ T) d\Omega = 0,$$

$$\int_\Omega (\nabla \omega \cdot \nabla \psi_2 + \sqrt{Ra}\ \frac{\partial \omega}{\partial x}\ T) d\Omega = 0,$$

$$\int_\Omega \omega T_t d\Omega + \sqrt{Ra}\int_\Omega \omega \left(\frac{\partial \psi_2}{\partial y}\frac{\partial T}{\partial x} + \left(\frac{\partial \psi_1}{\partial z} - \frac{\partial \psi_2}{\partial x}\right)\frac{\partial T}{\partial y} - \frac{\partial \psi_1}{\partial y}\frac{\partial T}{\partial z}\right) d\Omega + \int_\Omega \nabla \omega \cdot \nabla T d\Omega = 0.$$

The weak form of the velocity formulation in 2D is

$$\int_\Omega (\nabla \omega \cdot \nabla u + \sqrt{Ra}\ \frac{\partial \omega}{\partial y}\frac{\partial T}{\partial x}) d\Omega = 0,$$

$$\int_\Omega (\nabla \omega \cdot \nabla v - \sqrt{Ra}\ \frac{\partial \omega}{\partial x}\frac{\partial T}{\partial x}) d\Omega = 0.$$

The weak form of the velocity formulation in 3D is

Huang and Wellmann.

$$\int_\Omega (\nabla \omega \cdot \nabla u + \sqrt{Ra}\ \frac{\partial \omega}{\partial y}\frac{\partial T}{\partial x})d\Omega = 0,$$

$$\int_\Omega (\nabla \omega \cdot \nabla v - \sqrt{Ra}\ (\frac{\partial \omega}{\partial x}\frac{\partial T}{\partial x} + \frac{\partial \omega}{\partial z}\frac{\partial T}{\partial z}))d\Omega = 0,$$

$$\int_\Omega (\nabla \omega \cdot \nabla w + \sqrt{Ra}\ \frac{\partial \omega}{\partial y}\frac{\partial T}{\partial z})d\Omega = 0.$$

The weak form of the energy conservation equation is

$$\int_\Omega \omega T_t d\Omega + \sqrt{Ra}\int_\Omega \omega q \cdot \nabla T\ d\Omega + \int_\Omega \nabla \omega \cdot \nabla T d\Omega = 0.$$

We use the Crank-Nicolson time integration scheme and the time step Δt is defined such that the CFL number [Courant et al. (1967)] is less than one. The code is provided in https://github.com/pwhuang/beagle.

2.4 Quality Measures of Convective Heat Transfer

The Nusselt number is used to measure the quality of convective heat transfer in our simulations, and it is defined as the ratio of convective heat transfer and conductive heat transfer. Due to its simplicity and practical reasons, the Nusselt number is widely used in experiments as a quality measure of convection. The Nusselt number is

$$Nu = \frac{1}{h_1 h_2}\int_0^{h_2}\int_0^{h_1} \frac{\partial T}{\partial y}\Big|_{y=1}\ dxdz,$$

where h_1 and h_2 are the length (x-direction) and the depth (z-direction) of the box. This definition is analogous to Hewitt et al. (2014), except that they defined the Nusselt number using the heat flux on the bottom boundary.

2.5 Benchmark Problems

We present the following benchmark problem to validate our finite element implementation of the stream function formulation and the velocity formulation.

2.5.1 The Elder Problem

Elder studied convection caused by localized heating using the Hele-Shaw cell experiment and numerical methods [Elder, 1967b]. It is one of the benchmark problems in software such as FEFLOW [Trefry and Muffels (2007)], SUTRA [Voss (1984)] and HydroGeoSphere [Brunner and Simmons (2012)] [Simmons and Elder (2017)]. The boundary conditions of the Elder problem are defined in Figure 1.

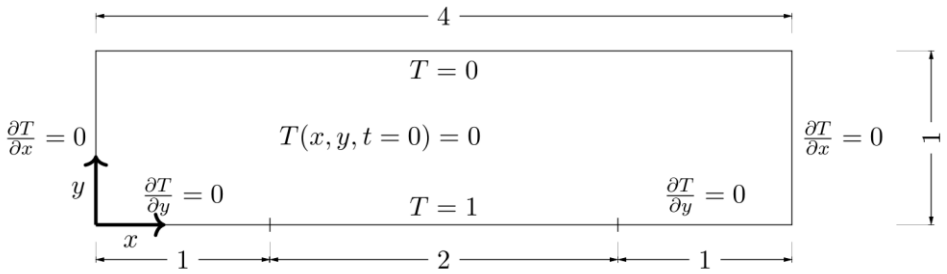

Figure 1: The boundary conditions of nondimensionalized temperature for the Elder problem.

We use the physical parameters of the Elder problem defined by Graf and Boufadel (2011), listed in Table 1.

Parameter	Value
Permeability (K)	1.21×10^{-10}m^2
Porosity (ϕ)	0.1
Reference fluid density (ρ_0)	996.526kg m^{-3}
Reference fluid viscosity (μ_0)	1.239×10^{-3}kg m^{-1}s^{-1}

Thermal conductivity of the fluid phase (k_f)	0.6 kg m s^{-3} K^{-1}
Thermal conductivity of the solid phase (k_s)	1.58889 kg m s^{-3} K^{-1}
Heat capacity of the fluid phase (c_f)	4184 m^2 s^{-2} K^{-1}
Heat capacity of the solid phase (c_s)	0 m^2 s^{-2} K^{-1}
Thermal expansion coefficient (α)	1.6163×10^{-4}
The temperature difference between the top and bottom boundary (ΔT)	8 K
Depth of the reservoir (d)	150 m

Table 1: Physical parameters used for the Elder problem. Modified from [Graf and Boufadel (2011)].

Combining the physical parameters, we have the Rayleigh number of 521.3. The time scale is roughly 200 years for one nondimensionalized time. We compare our simulations using the stream function formulation and the velocity formulation with the simulation results of HydroGeoSphere at 2, 5 and 10 years [Graf and Boufadel (2011)]. Since the velocity formulation sets up the other problems with injection and production wells easier, we only focus on benchmarking with the velocity formulation in the later sections.

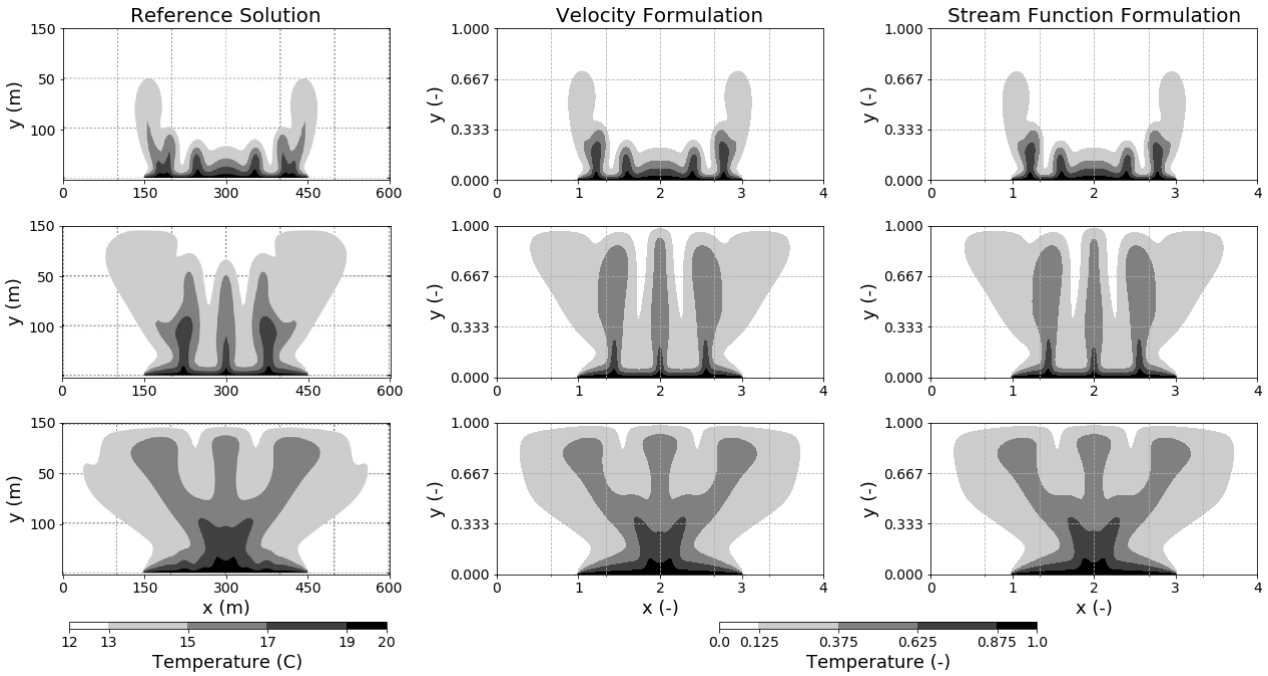

Figure 2: The comparison of temperature distribution between the simulations from the stream function formulation, the velocity formulation and the simulations of HydroGeoSphere [Graf and Boufadel (2011)].

2.5.2 Horne's Experiment

Horne (1975) performed experiments using a Hele-Shaw cell analogy with Rayleigh number equals to 1000 and 1600. One of the experiments is half heated from the bottom, like the Elder problem cut in half from the middle. Although this experiment is not a standard benchmark of the thermal-hydraulic problems, it is still worth testing to see if our code implementation can realize its unsteady oscillatory behavior. A direct quote from Horne (1975): "The pattern soon becomes largely unicellular and instead of irregular fluctuations the behavior is oscillatory, periodically generating 'tongues' of fluid in the ascending and descending regions of the flow." The results in Figure 3 also produced this oscillatory behavior and the 'tongues' are there.

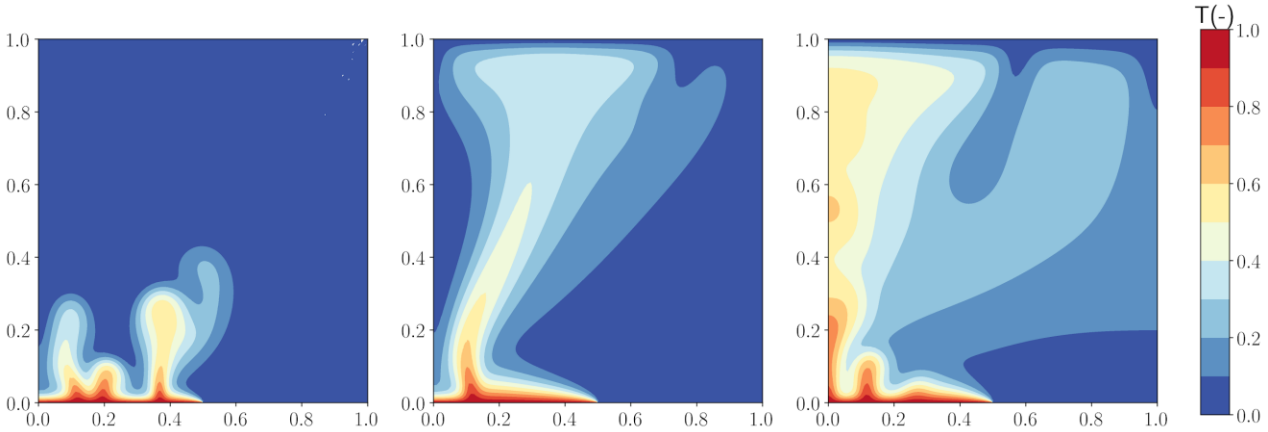

Figure 3: The temperature distribution of Horne's experiment, evolved with time from left to right. Simulated using the velocity formulation.

2.5.3 Beck's Box

Beck (1972) derived the preferred cellular mode during the onset of convection of a 3D box full of saturated porous media. We benchmark our code implementations using different boxes with lengths h_1 and depths h_2. We use the notation of $[h_1, h_2]$ to represent the box dimensions. The boxes we chose are [1.2, 1.2], [2.0, 0.5], [3.0, 1.0]. The Rayleigh number is set as 42.25, above the critical Rayleigh number, such that the system starts convecting. The initial condition of temperature is the conductive solution with a ±1% perturbation. The results are in Table 2, and they agree with Beck's analytical cellular modes.

Box type $[h_1, h_2]$	Critical Rayleigh number Ra_c	Beck's predicted cellular mode at Ra_c	Simulated cellular mode at $Ra = 42.25$
[1.2, 1.2]	40.553	(1, 1)	(1, 1)
[2.0, 0.5]	39.478	(2, 0)	(2, 0)
[3.0, 1.0]	39.478	(0, 1) or (3, 0)	(0, 1) or (3, 0)

Table 2: Comparison of Beck's cellular mode and the simulated cellular mode.

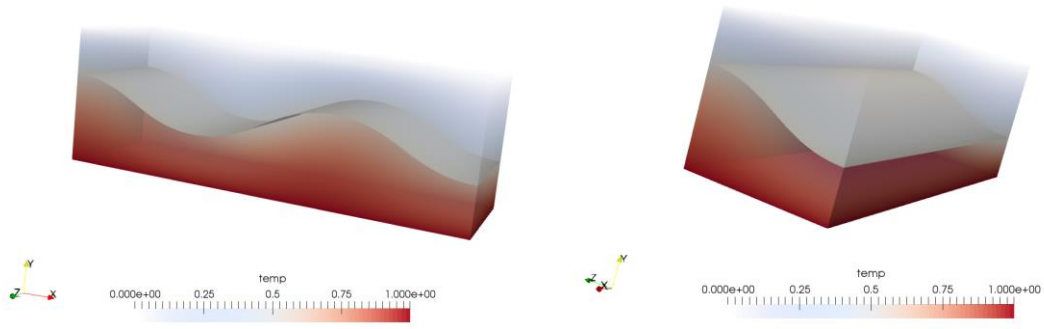

Figure 4: The temperature distribution of the box [3.0, 1.0]. The surface represents where the temperature equals to 0.5 (-). Left: (3, 0) mode. Right: (0, 1) mode.

2.6 The Nusselt-Rayleigh Relation

We test the hypothesis by simulating three boxes of different sizes that have two or three-dimensional preferred convection patterns during the onset of convection. The long boxes with sizes of [1.5, 1.0] and [2.3, 0.9] convect with a 2D convection pattern during the onset of convection, and the wide box [2.5, 1.5] convects with a 3D one. The three boxes are tested in the regions of $4\pi^2 \leq \mathrm{Ra} \leq 196$ with random initial conditions. The type of convection patterns and the Nusselt number are reported.

2.7 The Injection-Production Doublet Problem

We investigate the possibilities of perturbing the convection states by a typical strategy for geothermal energy production. Consider a doublet system that influences the velocity field of the reservoir. We claim that the pressure flux induced by the well can be defined as a point source of pressure flux on the top boundary. We approximate this point source of pressure flux by a Gaussian function, since

$$\delta(x - x_i) = \lim_{\sigma \to 0} exp(-\frac{(x-x_i)^2}{2\sigma^2}).$$

The effect of wells is, therefore, the sum of the Gaussian functions

$$v(x,z) = [q]\sum_{i=1}^{N} \quad A_i exp\left(-\frac{(x-x_i)^2}{2(\sigma_{xi})^2} - \frac{(z-z_i)^2}{2(\sigma_{zi})^2}\right),$$

where A is the amplitude of the Gaussian function, x_i and z_i are the coordinates of the center of the Gaussian hill, σ_{xi} and σ_{zi} defines how far the well influences the reservoir, and *N* is how many wells you have. The flow rate of the Gaussian functions is

$$Q_i = 2\pi[q]d^2 A_i \sigma_{xi}\sigma_{zi}.$$

Say we can introduce a flow rate of 10^{-3} m^3/sec for both the production and the injection wells to the reservoir. Using the material properties in Table 1, we have

$$A_i\sigma_{xi}\sigma_{zi} \approx 0.13.$$

We arbitrarily set $A_i = 13, \sigma_{xi} = \sigma_{zi} = 0.1$. We use the [1.5, 1.0] box with a Rayleigh number of 43.56, slightly above the critical Rayleigh number as an example, and set the initial condition to the (1, 1) convection pattern. We design two scenarios of the well placement. For scenario 1, we test if we can perturb the convection pattern to another state. We set the center of the effective injection at the coordinate (*x*=0.3, *y*=1.0, *z*=0.5), the center of effective production at (*x*=0.7, *y*=1.0, *z*=0.5), which will lead to a (1, 0) mode. For scenario 2, both wells are drilled into the downwelling zone of the convection pattern, where a lower temperature fluid is observed. We want to see whether the convection pattern changes, and hotter fluid can be pumped out. We visualize the boundary condition of the Darcy velocity *v* at the top boundary in Figure 3.

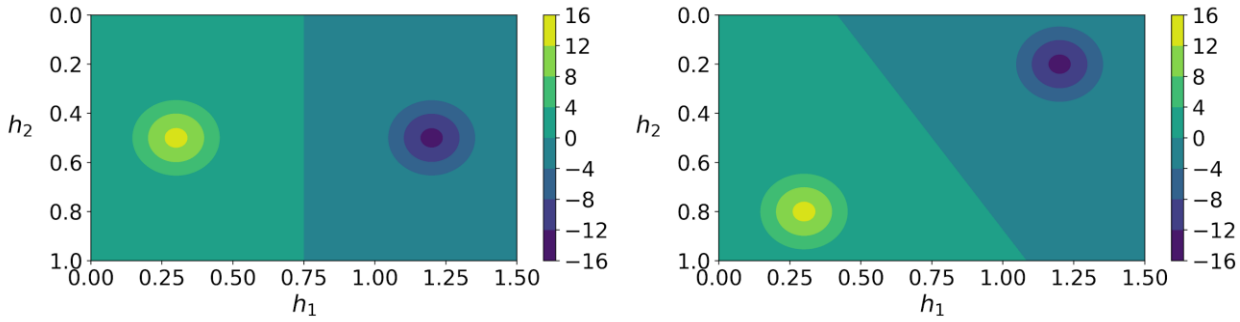

Figure 5: The prescribed velocity boundary condition of the doublet problem.

3. RESULTS

3.1 The Nusselt-Rayleigh Relation

We perform simulations of the boxes [1.5, 1.0], [2.3, 0.9] and [2.5, 1.5] while 42.25 < *Ra* < 196. See figure 6 for the results.

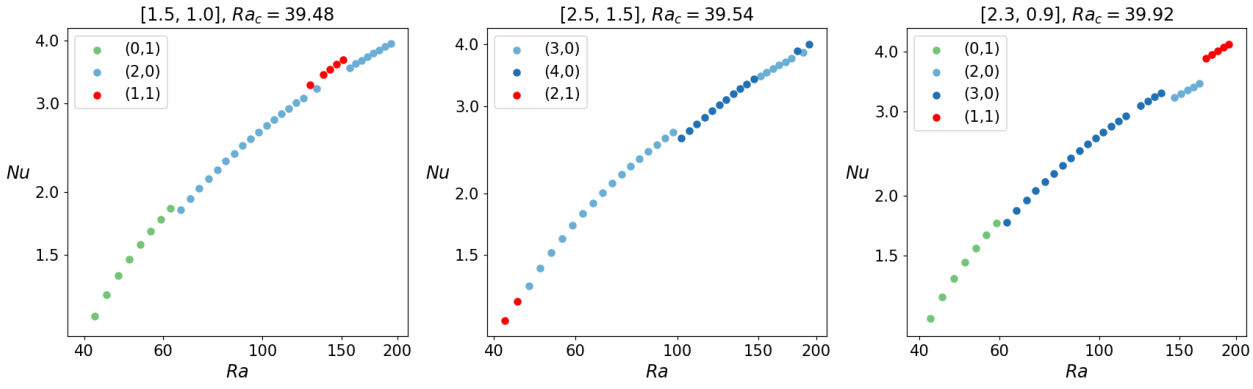

Figure 6: Compilation of the Nusselt-Rayleigh relation of the boxes [1.5, 1.0], [2.5, 1.5] and [2.3,0.9].

3.2 The Injection-Production Doublet Problem

To better understand the convection patterns, we perform a Fourier analysis to the convection temperature. The convection temperature is defined as

$$T_{convect} = T(x,y,z) - (1-y).$$

We define A_{mn} as the amplitude of $sin(\pi y)cos(m\pi x/h_1)cos(n\pi z/h_2)$. The solution can be approximated by the sum of these functions. We visualize the convection patterns in Figure 7 and 8. Figure 9 shows how the convection patterns change through time.

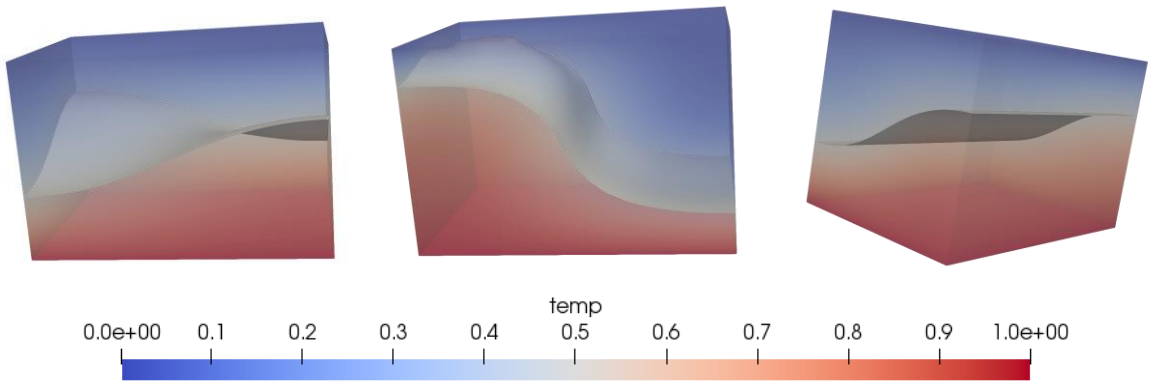

Figure 7: Scenario 1: The change of the convection pattern with respect to time. Left: The (1, 1) initial condition. Middle: The production state at time 0.2 (-). Right: The perturbed state of (0, 1).

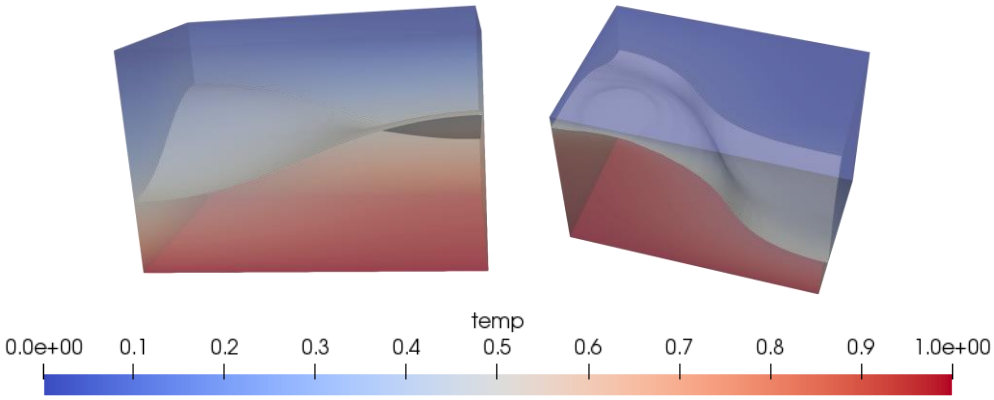

Figure 8: Scenario 2: The change of the convection pattern with respect to time. Left: The (1, 1) initial condition. Right: The perturbed state that consists of both (0, 1) and (1, 0) mode.

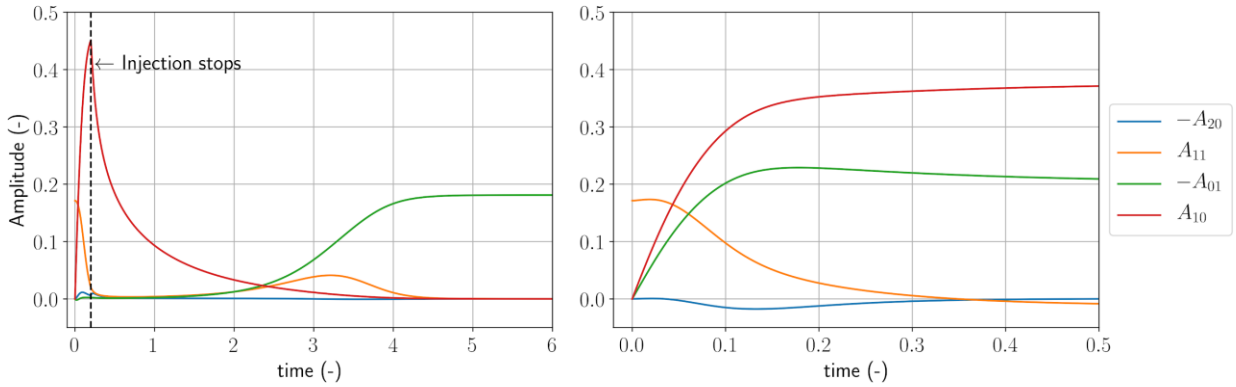

Figure 9: The phase diagram of the doublet problem. Left: Scenario 1. Right: Scenario 2.

4. DISCUSSION

4.1 The Nusselt-Rayleigh Relation

We showed that the state of the convection patterns does have an effect on the Nusselt number. When the boxes [1.5, 1.0] and [2.3, 0.9] are in the state of three-dimensional convection (1, 1), they have larger Nusselt numbers compared to the two-dimensional states. This observation agrees with Straus and Schubert (1979), that three-dimensional convection patterns have higher Nusselt number at $Ra > 97$. In any of the boxes, we observe jumps of Nusselt number between the different states of convection. To see how multiple steady-state solutions affect the Nusselt-Rayleigh relation, we plot the results of the three boxes over the compilation of Cheng (1979). The Nusselt number in the region of $Ra < 100$ shows some discrepancy, but it does not explain the scattering effect well. It can be

possible that some experimental settings of the porous boxes increase the critical Rayleigh number, therefore the onset of convection occurs at a higher Rayleigh number.

The result of $140 < Ra < 196$ shows a wide scattering range of the Nusselt number from 3.212 to 4.145. The first observation is that box sizes do have an effect on the Nusselt number. If we look closer, the boxes are in various convection states in the aforementioned region of Rayleigh number. Given the initial condition of random perturbation of temperature, the solution of our box system does not necessarily converge at the state of maximum heat transfer. Our results agree with the numerical simulations of Straus and Schubert (1979), that both two and three-dimensional convection cells could be obtained at $60 \leq Ra \leq 150$. Therefore, we conclude that multiple steady-states of convection patterns are a reason for the discrepancy of the Nusselt-Rayleigh relation.

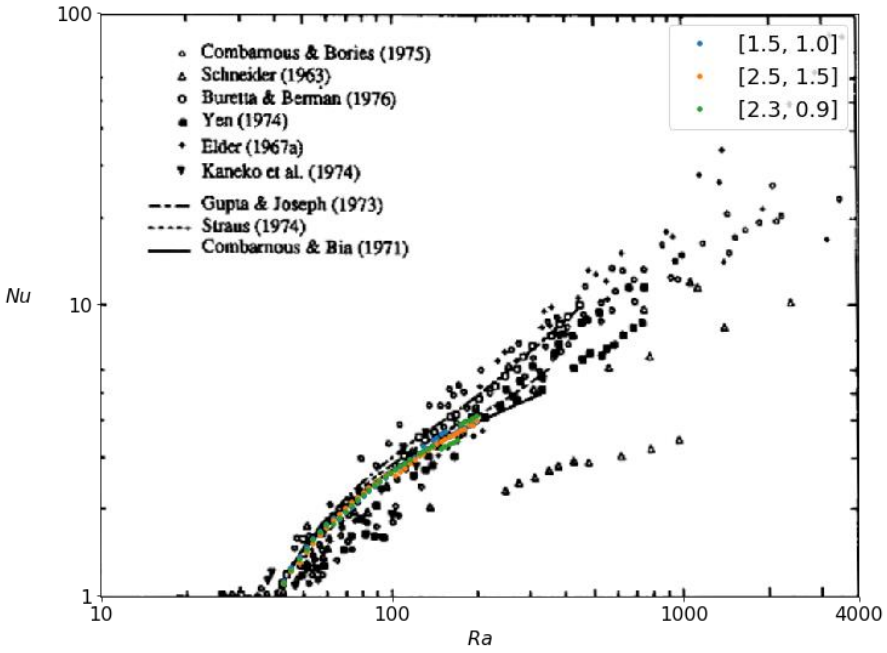

Figure 10: The Nusselt-Rayleigh relation of the boxes [1.5, 1.0], [2.3, 0.9] and [2.5, 1.5], plotted over the compilation of the Nusselt-Rayleigh relation from Cheng (1979).

4.2 The Injection-Production Doublet Problem

4.2.1 Scenario 1

Scenario 1 investigates how perturbing the velocity field for a relatively short time effect the convection state. When the doublet starts circulating, the amplitude of (1, 0) mode increases and the initial (1, 1) mode fades away. After the circulation stops, the amplitude of (1, 0) mode decreases exponentially. We observed that the amplitudes of both (1, 1) and (0, 1) mode start to increase, and eventually reservoir reaches a steady state of (0, 1) mode. Therefore, we claim that it is possible to change the convection pattern of a geothermal reservoir by the perturbation of the Darcy velocity.

4.2.2 Scenario 2

This scenario investigates whether we can reach a much favorable convective state if the wells are drilled into the downwelling region of the geothermal reservoir. The answer is simply yes. Applying constant circulation for 0.3 nondimensional time, the amplitude of the unfavorable state (1, 1) almost vanished. The convective state reached a combination of two states (1, 0) and (0, 1). This is a favorable state where the upwelling zone reaches the production well, and the downwelling zone reaches the injection well.

Recall that using the physical parameters in Table 1, one nondimensional time represents roughly 200 years. The time scale is proportional to reservoir depth squared. Therefore, if the reservoir depth is halved, we have one nondimensional time equals to 50 years, which is more manageable.

5. CONCLUSION

We use the Elder problem as a benchmark and show that the stream function and the velocity formulations are valid for solving problems of hydrothermal convection in porous media. Using the velocity formulation, we performed the three-box test. It allows us to explain how box sizes and multiple steady-states of convection patterns leads to the discrepancy of the Nusselt-Rayleigh relation in the region of $Ra < 196$.

The fact that

- multiple steady-states of convection patterns exist and
- different convection pattern leads to a different value of Nusselt number

tells us that a naturally convected geothermal reservoir may not be in its most efficient state of transferring heat to the surface. We used the doublet problem to show that it is possible to change the convection states from one another by perturbing the velocity field.

NOMENCLATURE

Ra	Rayleigh number
Ra_c	Critical Rayleigh number
Nu	Nusselt number
ρ_f	Density of fluid
ρ_s	Density of solid
Φ	Porosity of the reservoir
ψ	Stream Function
T	Temperature
p	Pressure
q	Darcy velocity, vector
u	The x component of the Darcy velocity
v	The y component of the Darcy velocity
w	The z component of the Darcy velocity
K	Permeability
μ	Dynamic viscosity of fluid
d	Depth of the reservoir
c	Heat Capacity
α	Thermal expansion coefficient of fluid
g	Gravity
$[h_1, h_2]$	Box sizes. h_1 is the length in the x-direction. h_2 is the length in the y-direction.
(m, n)	Convection pattern or convection modes
ω	Test function

ACKNOWLEDGEMENT

The authors gratefully acknowledge the computing time granted through JARA-HPC on the supercomputer JURECA at Forschungszentrum Jülich. Since the first author has been studying in the Geothermal Energy and Geofluids group from August 2018, he thanks the Werner Siemens Foundation for their endowment of the Geothermal Energy and Geofluids group at the Institute of Geophysics, ETH Zürich.

REFERENCES

Barenblatt, G.: Scaling, Self-similarity, and Intermediate Asymptotics: Dimensional Analysis and Intermediate Asymptotics, Cambridge Texts in Applied Mathematics, Cambridge University Press, (1996).

Bear, J.: Dynamics of Fluids in Porous Media, American Elsevier Publishing, (1972).

Beck, J.L.: Convection in a Box of Porous Material Saturated with Fluid, The Physics of Fluids, 15(8), (1972), 1377-1382.

Bejan, A.: Convection Heat Transfer, John Wiley & Sons, (2013).

Börsing, N., Wellmann, J.F., Niederau, J., and Regenauer-Lieb, K.: Entropy Production in a Box: Analysis of Instabilities in Confined Hydrothermal Systems, Water Resources Research, 53(9), (2017), 7716-7739.

Brunner P., Simmons, C.T.: HydroGeoSphere: A Fully Integrated, Physically Based Hydrological Model, Groundwater, 50(2), (2012), 170-176.

Buretta, R.J., and Berman, A.S.: Convective Heat Transfer in a Liquid Saturated Porous Layer, Journal of Applied Mechanics, 43(2), (1976), 249-253.

Cheng, P.: Heat Transfer in Geothermal systems, Advances in Heat Transfer, 14, (1979), 1-105.

Combarnous, M.A., and Bories, S.A.: Hydrothermal Convection in Saturated Porous Media, Advances in Hydroscience, 10, (1975), 231-307.

Combarnous, M.A., and Bia, P.: Combined Free and Forced Convection in Porous Media, Society of Petroleum Engineers Journal, 11(4), (1971), 399-405.

Costa, V.A.F.: On Natural Convection in Enclosures Filled with Fluid-Saturated Porous Media Including Viscous Dissipation, International Journal of Heat and Mass Transfer, 49(13-14), (2006), 2215-2226.

Courant, R., Friedrichs, K., and Lewy, H.: On the Partial Differential Equations of Mathematical Physics, IBM Journal of Research and Development, 11(2), (1967), 215-234.

Elder, J.W.: Steady Free Convection in a Porous Medium Heated from Below, Journal of Fluid Mechanics, 27(1), (1967a), 29-48.

Elder, J.W.: Transient Convection in a Porous Medium, Journal of Fluid Mechanics, 27(3), (1967b), 609-623.

Florio, B.J.: The Interaction of Convection Modes in a Box of a Saturated Porous Medium, Journal of Engineering Mathematics, 86(1), (2014), 71-88.

Fowler, A.C.: Mathematical Models in the Applied Sciences, Cambridge University Press, (1997).

Gaston, D., Newman, C., Hansen, G., and Lebrun-Grandié, D.: MOOSE: A Parallel Computational Framework for Coupled System of Nonlinear Equations, 239(10), (2009), 1768-1778.

Goldberg, D.: What Every Computer Scientists should know about Floating-point Arithmetic, ACM Computing Surveys, 23(1), (1991), 5-48.

Grant, M.A., and Bixley, P.F.: Geothermal Reservoir Engineering, Second Edition, Academic Press, (2011).

Graf, T., and Boufadel, M.C.: Effect of Viscosity, Capillarity and Grid Spacing on Thermal Variable-density Flow, Journal of Hydrology, 400(1-2), (2011), 41-57.

Grodzka-Łukaszewska, M., Nawalany, M. and Zijl, W.: A Velocity-Oriented Approach for Modflow, Transport in Porous Media, 119(2), (2017), 373-390.

Gupta, V.P., and Joseph, D.D.: Bounds for Heat Transport in a Porous Layer, Journal of Fluid Mechanics, 57(3), (1973), 491-514.

Hewitt, D.R., Neufeld, J.A., and Lister, J.R.: High Rayleigh Number Convection in a Three-dimensional Porous Medium, Journal of Fluid Mechanics, 748, (2014), 879-895.

Holst, P.H., and Aziz, K.: Transient Three-dimensional Natural Convection in Confined Porous Media, International Journal of Heat and Mass Transfer, 15(1), (1972), 73-90.

Horne, R.N.: Transient Effects in Geothermal Convective Systems, Ph.D. thesis, The University of Auckland, (1975).

Horne, R.N.: Three-dimensional Natural Convection in a Confined Porous Medium Heated from below, Journal of Fluid Mechanics, 92(4), (1979), 751-766.

Kaneko, T., Mohtadi, M.F., and Aziz, K.: An Experimental Study of Natural Convection in Inclined Porous Media, International Journal of Heat and Mass Transfer, 17, 485-496.

Langtangen, H.P. and Pedersen, G.K.: Scaling of Differential Equations, Springer International Publishing, (2016).

Lipsey, L., Pluymaekers, M., Goldberg T., van Oversteeg, K., Ghazaryan, L., Cloetingh, S., and van Wees, J.D.: Numerical Modelling of Thermal Convection in the Luttelgeest Carbonate Platform, the Netherlands, Geothermics, 64, (2016), 135-151.

Lister C.R.B.: An Explanation for the Multivalued Heat Transport Found Experimentally for Convection in a Porous Medium, Journal of Fluid Mechanics, 214, (1990), 287-320.

Niederau, J., Ebigbo, A., Marquart, G., Arnold, J., and Clauser, C.: On the Impact of Spatially Heterogeneous Permeability on Free Convection in the Perth Basin, Australia, Geothermics, 66, (2017), 119-133.

Nield, D., and Bejan, A.: Convection in Porous Media, Springer International Publishing, (2017).

Otero, J., Dontcheva, L.A., Johnston, H., Worthing, R.A., Kurganov, A., Petrova, G., and Doering, C.R.: High-Rayleigh-number Convection in a Fluid-saturated Porous Layer, Journal of Fluid Mechanics, 500, (2004), 263-281.

Schneider, K.: Investigation of the Influence of Free Thermal Convection on Heat Transfer Through Granular Material, Proceedings of the 11th International Congress of Refrigeration, (1963), 247-253.

Simmons, C.T., and Elder, J.W.: The Elder Problem, Groundwater, 55(6), (2017), 926-930.

Straus, J.M.: Large Amplitude Convection in Porous Media, Journal of Fluid Mechanics, 64(1), (1974), 51-63.

Straus, J.M., and Schubert, G.: Three-dimensional Convection in a Cubic Box of Fluid-saturated Porous Material, Journal of Fluid Mechanics, 91(1), (1979), 155-165.

Trefry, M.G., and Muffels, C.: FEFLOW: A Finite-Element Ground Water Flow and Transport Modeling Tool, Groundwater, 45(5), (2007), 525-528.

Vadasz, P.: Heat Flux Dispersion in Natural Convection in Porous Media, International Journal of Heat and Mass Transfer, 53(17-18), (2010), 3394-3404.

Voss, C.I.: A Finite-Element Simulation Model for Saturated-unsaturated, Fluid-density-dependent Ground-water Flow with Energy Transport or Chemically-reactive Single-species Solute Transport, Water-Resources Investigations Report, (1984).

Yen, Y.C.: Effects of Density Inversion on Free Convective Heat Transfer in Porous Layer Heated from Below, International Journal of Heat and Mass Transfer, 17(11), 1349-1356.